Journal of Biomedical Optics

BiomedicalOptics.SPIEDigitalLibrary.org

Review of short-wave infrared spectroscopy and imaging methods for biological tissue characterization

Robert H. Wilson
Kyle P. Nadeau
Frank B. Jaworski
Bruce J. Tromberg
Anthony J. Durkin

SPIE.

Journal of Biomedical Optics 20(3), 030901 (March 2015)

REVIEW

Review of short-wave infrared spectroscopy and imaging methods for biological tissue characterization

Robert H. Wilson,[a] Kyle P. Nadeau,[a] Frank B. Jaworski,[b] Bruce J. Tromberg,[a] and Anthony J. Durkin[a,*]
[a]University of California, Irvine, Beckman Laser Institute, 1002 Health Sciences Road, Irvine, California 92612, United States
[b]Raytheon Vision Systems, 75 Coromar Drive, Goleta, California 93117, United Sates

Abstract. We present a review of short-wave infrared (SWIR, defined here as ~1000 to 2000 nm) spectroscopy and imaging techniques for biological tissue optical property characterization. Studies indicate notable SWIR absorption features of tissue constituents including water (near 1150, 1450, and 1900 nm), lipids (near 1040, 1200, 1400, and 1700 nm), and collagen (near 1200 and 1500 nm) that are much more prominent than corresponding features observed in the visible and near-infrared (VIS-NIR, defined here as ~400 to 1000 nm). Furthermore, the wavelength dependence of the scattering coefficient has been observed to follow a power-law decay from the VIS-NIR to the SWIR region. Thus, the magnitude of tissue scattering is lower at SWIR wavelengths than that observed at VIS or NIR wavelengths, potentially enabling increased penetration depth of incident light at SWIR wavelengths that are not highly absorbed by the aforementioned chromophores. These aspects of SWIR suggest that the tissue spectroscopy and imaging in this range of wavelengths have the potential to provide enhanced sensitivity (relative to VIS-NIR measurements) to chromophores such as water and lipids, thereby helping to characterize changes in the concentrations of these chromophores due to conditions such as atherosclerotic plaque, breast cancer, and burns. [DOI: 10.1117/1.JBO.20.3.030901]

Keywords: short-wave infrared; near-infrared; tissue spectroscopy; multispectral imaging; tissue properties; optical properties; absorption coefficient; scattering coefficient.

Paper 140807VR received Dec. 10, 2014; accepted for publication Feb. 24, 2015; published online Mar. 24, 2015.

1 Introduction

Spectroscopic and imaging techniques consisting of the delivery of light to a biological tissue sample and detection of the diffusely reflected or transmitted light from the sample are well-established means of interrogating tissue composition, structure, and function.[1,2] Most tissue optics research to date has employed wavelengths in the visible and near-infrared regions of the spectrum (VIS-NIR, defined here as ~400 to 1000 nm). A primary goal of many VIS-NIR studies is to characterize the functional status of a tissue by measuring the concentration of oxygenated hemoglobin [primary absorption peak near 414 nm and secondary absorption peaks near 543 and 577 nm (Ref. 3)] and deoxygenated hemoglobin [primary absorption peak near 433 nm and secondary absorption peak near 556 nm (Ref. 3)]. In addition, some studies have employed signals detected at the long wavelength edge of the NIR (900 to 1000 nm) to extract parameters related to tissue water and lipid concentrations, because water and lipid have small absorption features near 970 (Ref. 4) and 930 nm,[5] respectively. These studies have provided information about changes in water fraction due to edema in burns[6] and changes in relative amounts of hemoglobin, water, and lipid content in breast tumors.[1] However, the VIS-NIR region (as defined above) does not include many of the prominent absorption peaks of water and lipids.

To obtain additional quantitative information about biological tissue constituents, it may be advantageous to extend optical measurements into the short-wave IR (SWIR) spectral region (defined here as ~1000 to 2000 nm). The SWIR regime includes prominent absorption peaks of water, lipids,[4,5,7] and collagen[8] (Fig. 1).

For lipids, the absorption peaks at 920, 1040, 1210, 1730, and 1760 nm are associated with overtones of the stretching vibrational mode of the C-H bond.[9,10] The 920 and 1210 nm peaks are associated with the second overtone of C-H stretching,[10,11] while the 1730 and 1760 nm peaks are associated with the first overtone of C-H stretching.[10–12] The absorption peak near 1430 nm can be attributed to the first overtone of O-H stretching.[10,12] Different types of lipids, such as cholesterol, cholesterol esters, phospholipids, and triglycerides, are known to have absorption spectra that are similar to each other, with distinctive peaks in the SWIR region.[9]

For collagen, the absorption spectrum has a peak at 1200 nm from the second overtone of C-H stretching,[11] a peak near 1500 nm from a combination band of CH_2 stretching and non-stretching,[13] a peak at 1725 nm due to symmetric and asymmetric stretching bands from the CH_2 bond,[11] and a shoulder at 1690 nm from the first overtone of CH_3 stretching.[11]

For water, the absorption peaks at 970 and 1180 nm are from a vibrational overtone of the O-H bond.[9] The peak near 1430 nm is due to the first overtone of O-H stretching,[10,12] the peak near 1930 nm is due to an O-H stretch/deformation combination,[10,12] and the peak near 1975 nm is due to an O-H bend second overtone.[10]

*Address all correspondence to: Anthony J. Durkin, E-mail: adurkin@uci.edu

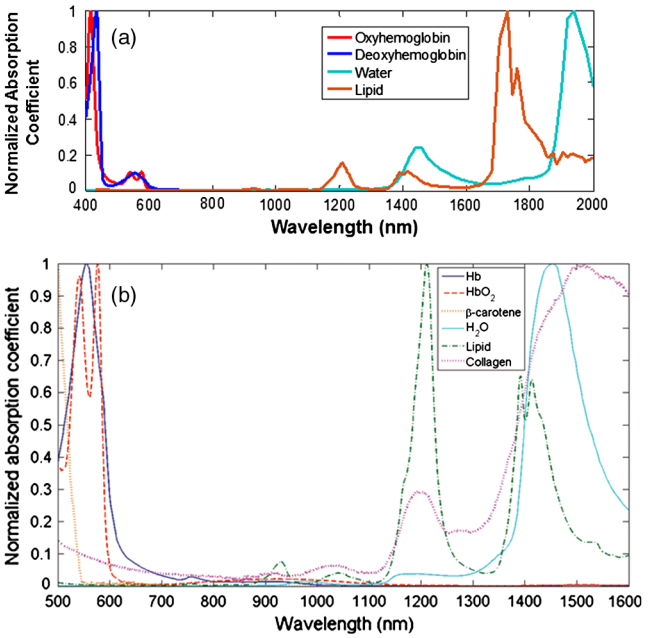

Fig. 1 (a) Absorption coefficients of oxygenated and deoxygenated hemoglobin, water, and lipid in the visible and near-infrared (VIS-NIR) (defined here as ~400 to 1000 nm) and short-wave infrared (SWIR) (defined here as ~1000 to 2000 nm) regions, obtained from Refs. 3, 4, and 7, with each spectrum normalized to its maximum value for ease of comparison. Both water and lipid have prominent absorption peaks in the SWIR, despite not having many notable features in the VIS or NIR regions. These spectra suggest that SWIR measurements have the potential to provide tissue composition information that is not nearly as readily available in the VIS-NIR. (b) Absorption coefficients, from Ref. 8, of the same tissue constituents as in (a), from 500 to 1600 nm, with collagen and beta-carotene added, with each spectrum normalized to its maximum value (reproduced with permission). Collagen exhibits a major SWIR absorption peak near 1500 nm as well as secondary absorption peaks near 1050 and 1200 nm; most of this information content is not accessible with VIS-NIR measurements.

The absorption coefficient of water is over 60 times greater at 1440 nm than at the 970-nm NIR peak and over 260 times greater at 1940 nm than at the 970-nm NIR peak.[4] Similarly, the absorption coefficient of lipid is over 12 times greater at 1210 nm than at the 930-nm NIR peak, over 8 times greater at 1390 nm than at the 930-nm NIR peak, and over 80 times greater at 1730 nm than at the 930-nm NIR peak.[7] Absorption peaks from cholesterol are seen near 1200, 1400, and 1750 nm,[14] suggesting that the SWIR wavelength range has the potential to capture information about cholesterol that is unavailable in the VIS-NIR. Therefore, measurements at SWIR wavelengths could provide improved sensitivity to the water and lipid content of biological tissues. This increased sensitivity is likely to be important for applications such as assessment and monitoring of burns (which are marked by changes in water fraction due to edema), characterization of atherosclerotic plaque (which can be classified according to changes in lipid content), and detection and monitoring of cancer (which is known to cause changes in the structural and biochemical contents of tissue). Specific studies related to the aforementioned applications will be discussed in the body of this paper.

Here, we present a review of SWIR techniques that have been employed to characterize biological tissues. Early SWIR studies largely consisted of reflectance and transmittance measurements on thin slices of *ex vivo* tissue, using integrating sphere setups.[15–20] More recently, SWIR measurements have been performed with fiber-probe-based setups,[21–28] which have the portability and flexibility required to enable wavelength-resolved and time-resolved measurements of *in vivo* tissues. Most clinically compatible SWIR tissue measurements have only been tested on *ex vivo* samples, but some groups[9,29,30] have begun to perform *in vivo* SWIR imaging of biological tissues. These initial studies demonstrate that SWIR measurements of tissue can provide a more spectral-information-rich dataset for quantitative characterization of *in vivo* tissue structure and function, including increased spectral information content about water and lipid absorptions that are not available in the VIS-NIR region. We will summarize several of these studies in the following sections.

2 Integrating Sphere-Based Short-Wave Infrared Measurements

Several studies have measured *ex vivo* tissue absorption $[\mu_a(\lambda)]$ and reduced scattering $[\mu_s'(\lambda)]$ coefficients in the SWIR region using integrating sphere setups.[15–20] Integrating sphere methods have been widely employed in tissue optics to measure tissue optical property spectra (e.g., Ref. 31). These methods involve two measurements: a diffuse transmittance measurement, where the sample is placed at the entrance port of the sphere, and a diffuse reflectance measurement, where the sample is located at the exit port at the back of the sphere. An unscattered (collimated) transmittance measurement can also be performed, if desired, to separate the reduced scattering coefficient into the scattering coefficient $[\mu_s(\lambda)]$ and the anisotropy factor $[g(\lambda)]$. In the studies that we review here, light collected by the integrating sphere setup was sent to detectors that are sensitive to SWIR wavelengths [e.g., indium gallium arsenide (InGaAs)]. The reflectance $[R(\lambda)]$ and transmittance $[T(\lambda)]$ measurements are then used in combination with a model of light propagation, such as inverse adding doubling,[31] to enable the determination of the tissue absorption and reduced scattering coefficients.

Du et al.[15] used an integrating sphere setup employing a tunable light source consisting of a tungsten lamp and a monochromator to measure the optical properties of *ex vivo* porcine dermis in the 900- to 1500-nm range, as skin optical properties had not been well characterized in this range prior to this study. The measured reflectance and transmittance spectra both exhibited prominent dips in the 1400 to 1500 nm ranges, attributable to an overtone of the O-H stretch vibrational mode of water,[32] a result that corresponded with the trend in the reported $\mu_a(\lambda)$, which was over 10 times greater at 1450 nm than at 980 nm.

Zamora-Rojas et al.[16] used a double integrating sphere setup to measure *ex vivo* porcine skin from 1150 to 2250 nm to investigate metrics for pork quality assessment. These measurements employed a supercontinuum laser (460 to 2400 nm), a monochromator (450 to 2800 nm), and InGaAs detectors.[17] The reflectance, transmittance, and collimated transmittance all exhibited local minima near 1450 and 1950 nm. The value of $\mu_a(\lambda)$ reached a local maximum of ~3 mm^{-1} near 1450 nm, but the values of $\mu_a(\lambda)$ from 1880 to 2040 nm could not be determined because high absorption within the samples resulted in measured values of transmittance, $T(\lambda)$, to be near zero in this range. Overall, the absorption spectra of the skin tissue were found to be primarily composed of features from water and

the scattering coefficient was found to decrease with increasing wavelength.

Troy and Thennadil[18] used a double integrating sphere setup with a tungsten-halogen light source and InGaAs detectors to measure human skin (22 samples, 14 subjects) from 1000 to 2200 nm. The study was designed to characterize the optical properties of skin across a wide wavelength range, in order to ultimately determine which window(s) of this range would be most suitable for the use of a noninvasive glucose detection instrument and to develop a quantitative method to correct glucose measurements for the effects of tissue absorption and scattering. The measured $\mu_a(\lambda)$ was in agreement with a theoretical calculation for 70% water. However, data could not be obtained in the range of 1900 to 2040 nm due to high water absorption. The measured $\mu_s'(\lambda)$ was modeled with a power law of the form $\mu_s'(\lambda) = (2 \times 10^4\ \text{mm}^{-1})(\lambda/\lambda_0)^{-1.5}$, where $\lambda_0 = 1$ nm. Over the 1000- to 2200-nm window, $\mu_s'(\lambda)$ varied from 3 to 16 cm^{-1}. In addition, the $\mu_s'(\lambda)$ value from 1000 to 1800 nm was found to correlate inversely with age, a result potentially attributable to age-related decreases in cell density. Overall, the study succeeded in quantifying the absorption and scattering of human skin in the SWIR regime and determined that a 2% Intralipid solution could serve as an effective tissue simulating phantom from 1000 to 2200 nm. These results can be employed in future studies to motivate instrumentation and algorithm design for accurate, noninvasive SWIR-based *in vivo* glucose measurements.

Bashkatov et al.[19] used an integrating sphere setup with a halogen lamp and spectrometer for *ex vivo* measurements of human tissues (skin, subcutaneous adipose, and mucosal) from 400 to 2000 nm. The measurement of subcutaneous adipose tissue was motivated by the goal of developing optical techniques for treating conditions such as obesity. The measurements of skin and mucosal tissue were motivated by the need for improved dosimetry during photodynamic therapy of disease (using 850, 980, and 1064 nm light sources[33]) in tissues such as the bladder, colon, esophagus, and maxillary sinus. The absorption spectra of the tissues had peaks near 1200, 1430, 1750, and 1925 nm [Fig. 2(a)], attributed to water and lipids. The $\mu_s'(\lambda)$ of skin [Fig. 2(b)] was modeled as a sum of two power-law terms: $\mu_s'(\lambda) = (1.1 \times 10^{11})\lambda^{-4} + (7.37)\lambda^{-0.22}\ \text{mm}^{-1}$, with the λ^{-4} term modeling Rayleigh scattering and the $\lambda^{-0.22}$ term modeling Mie scattering. The reduced scattering coefficients of mucosal and subcutaneous adipose tissues were approximated with single-power-law models. A key conclusion of this study was that the power-law behavior of $\mu_s'(\lambda)$ extended into the SWIR wavelength range, demonstrating that the tissue scattering continues to decrease monotonically in this regime.

Friebel et al.[20] used an integrating sphere setup with a cuvette to measure the optical properties of human red blood cells in saline in the range 250 to 2000 nm. The study aimed to characterize the optical properties of this suspension under different oxygenation levels in order to determine how $\mu_a(\lambda)$, and possibly $\mu_s(\lambda)$ and $g(\lambda)$, are influenced by oxygenation. The measured $\mu_a(\lambda)$ was found to contain few features of hemoglobin at wavelengths longer than 1100 nm. This result is consistent with the fact that the oxy-hemoglobin absorption decreases by a factor of ~50 at 1000 nm, relative to its 576-nm absorption peak, and that the deoxy-hemoglobin absorption decreases by a factor of ~250 at 1000 nm, relative to its 556 nm absorption peak.[3] The measured $\mu_s(\lambda)$ followed a power-law model with an exponent (b) of −0.93 for wavelengths in the NIR and SWIR

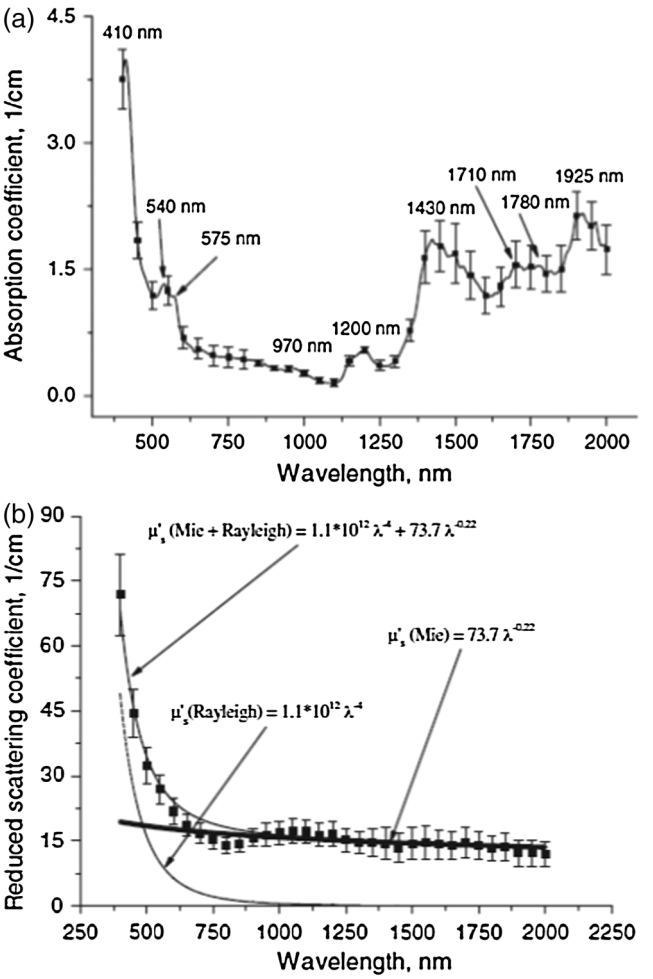

Fig. 2 (a) Absorption spectrum $\mu_a(\lambda)$ from 400 to 2000 nm for human skin tissue ($N = 21$ samples) measured *ex vivo* in Ref. 19, with prominent absorption peaks labeled. (b) Reduced scattering spectrum $\mu_s'(\lambda)$ from 400 to 2000 nm for the same human skin tissue dataset as in (a), modeled as a sum of Rayleigh scattering (λ^{-4}, most prominent at visible wavelengths) and Mie scattering ($\lambda^{-0.22}$, most prominent at NIR and SWIR wavelengths). Error bars represent standard deviation over the number of samples. Notable water and lipid absorption peaks are present throughout a large portion of the SWIR region, and the reduced scattering spectrum can be approximated by a Mie scattering power law in the SWIR region. These spectra suggest that SWIR measurements can be employed to detect spectral signatures of water and lipid in skin and that the power-law behavior of the reduced scattering coefficient extends into the SWIR regime. (Figure

regions. The measured $g(\lambda)$ was nearly flat (~0.96 to 0.98) from 1000 to 1750 nm, but it was observed to dip below 0.9 at 1900 nm, the location of the most prominent SWIR water absorption peak. The $\mu_s'(\lambda)$ spectrum of the suspension exhibited a corresponding peak at 1900 nm (an increase by roughly a factor of 2, relative to its value at 1750 nm). However, it is possible that these effects may be artifacts of crosstalk between absorption and scattering in the data analysis procedure.

Anderson et al.[34] used an integrating sphere spectrophotometer setup to measure the absorption spectra of human subcutaneous fat. A goal of these measurements was to identify absorption peaks of lipid in the SWIR regime for use in selective photothermolysis.[35] Prominent fat absorption peaks were observed at 1210 and 1720 nm; at both of these wavelengths,

the absorption from fat exceeded the absorption of water. This result suggests that the lipids have notable spectral features in the SWIR regime that can be selectively targeted due to their spectral separation from the prominent absorption peaks of water.

Martin[36] examined the SWIR absorption of human skin *in vivo* by placing a detector, comprised of a spectrograph and an integrating sphere, directly onto the tissue surface. The detector measured reflectance from 1200 to 2400 nm; prominent skin absorption peaks near 1450, 1775, and 1900 nm corresponded to the absorption peaks of water in those spectral regions. Minima near 1875, 1890, 1910, and 1925 nm in the second derivative of the skin reflectance spectrum were attributed to different binding states of water, and the relative intensities of the reflectance signals at these bands were observed to change in response to occlusion and variation in relative humidity.

The main conclusions of the SWIR integrating sphere studies were: (1) the tissue scattering coefficient obeyed a power law over the SWIR wavelength region and the NIR wavelength region, and (2) tissue absorption coefficients showed prominent water- and lipid-related absorption features in the SWIR region. These measurements highlighted prominent spectral features of tissue absorption and scattering in the SWIR regime; however, the integrating sphere method is fundamentally limited to *ex vivo* tissue samples that are of appropriate thickness to enable collection of both diffuse reflectance and diffuse transmittance.

3 Fiber-Probe-Based Short-Wave Infrared Measurements

SWIR measurements have also been performed using "point" probe geometries that employ optical fibers[21–28] to obtain measurements of reflectance collected over small localized tissue volumes that are adjacent (within microns to millimeters) to the point of contact. The interrogation volume of these probes is defined in part by the spacing between the source and detector fibers.[37] Fiber-probe-based methods enable interrogation of *ex vivo* and *in vivo* intact tissues because, unlike integrating sphere setups, these methods typically employ measurement geometries that can be approximated as semi-infinite by radiative transport modeling approaches and thus do not require concurrent reflectance and transmittance measurements or an *a priori* knowledge of sample thickness. These fiber-based systems can also be employed preclinically or clinically due to their portable, flexible, and minimally invasive nature. Fiber-based methods have shown that the use of steady-state and time-resolved SWIR information contents related to water and lipids can enable improved detection of diseases such as atherosclerosis and cancer, as will be reviewed below. One of these groups[21] directly showed that adding SWIR information content to VIS-NIR information content can provide improved confidence levels for cancer detection (relative to using VIS-NIR alone). However, it is important to remember that the sampled volume of tissue is a function of the source-detector separation of the fiber probe. Therefore, for layered tissues (such as skin), the reflectance spectra will be influenced by a combination of the optical properties of the different tissue layers, weighted according to the percentage of photon path spent in each layer (which is in part defined by the source-detector separation).

Within the context of cardiovascular disease detection, there have been a number of investigations that suggest the potential of SWIR-derived information to enhance understanding related to pathologic changes in tissue composition. Wang et al.[22] used a fiber probe and spectrometer to measure the absorbance [defined as log(1/reflectance)] of *ex vivo* carotid atherosclerotic plaques obtained from 25 patients (Fig. 3). Lipid-to-protein ratios in the spectral regions from 1130 to 1260 nm, 1620 to 1820 nm, and 2200 to 2330 nm were employed to distinguish between vulnerable, stable, and intermediate plaques. Moreno et al.[23] performed *ex vivo* reflectance measurements from 1100 to 2200 nm on 199 human aorta samples obtained at autopsy. Multivariate statistical analysis was carried out to classify the spectra, and principal components of these data were employed for differentiating stable plaque from vulnerable plaque.

Nachabé et al.[24] employed a fiber probe to measure *ex vivo* porcine tissues (fat, muscle, and white matter) from 900 to 1600 nm to validate a noninvasive, clinically compatible method for extracting water and lipid volume fractions from tissue. In a related study, Nachabé et al.[21] directly compared two fiber-probe-based optical spectroscopic methods for obtaining tissue water and lipid volume fractions: one method employing only VIS-NIR wavelengths (500 to 1000 nm) and other method including SWIR wavelengths in addition to VIS-NIR (500 to 1600 nm). These methods involved both measuring the reflectance spectrum of the tissue and modeling the reflectance spectrum as a function of the wavelength-dependent absorption and scattering coefficients of the tissue. The absorption coefficient was represented as a linear combination of all the absorbing species in the tissue, weighted according to their respective volume fractions. These two methods were employed to measure *ex vivo* porcine fat and muscle from 500 to 1600 nm (with the VIS-NIR-SWIR technique using silicon and InGaAs spectrometers in tandem).[21] The confidence levels associated with the water and lipid volume fractions obtained over the entire 500- to 1600-nm range were four times higher than those obtained from only 500 to 1000 nm.[21]

The results of Ref. 21 were then used by Nachabé et al.[8] to develop a breast cancer detection method employing optical spectroscopic measurements of *ex vivo* human breast tissues from 500 to 1600 nm (Fig. 4) to distinguish between adipose tissue, glandular tissue, fibroadenoma, invasive carcinoma, and ductal carcinoma *in situ* (DCIS). The water volume fraction was statistically significant for distinguishing fibroadenoma

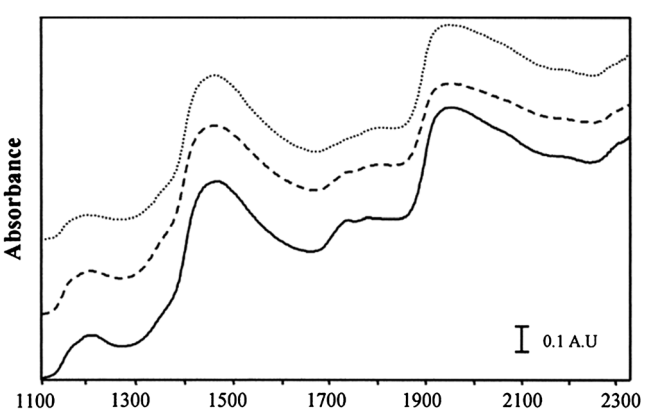

Fig. 3 SWIR absorbance spectra [unitless, defined as 1/log(reflectance)] of human carotid atherosclerotic plaques (fibrous, dotted line; calcified, dashed line; and soft, solid line), measured *ex vivo* using a fiber probe and spectrometer.[22] The spectra exhibit features of absorption from water (peaks near 1450 and 1950 nm) and lipids (peak near 1200 nm). This work suggests that SWIR may have the potential to differentiate between vulnerable plaque and more stable forms of plaque. (Figure reproduced with permission.)

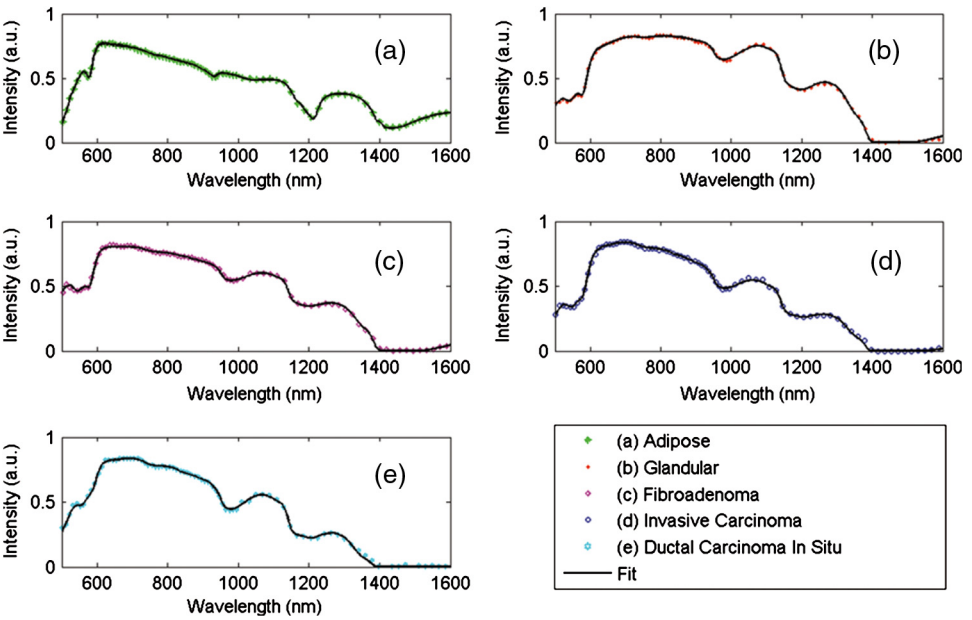

Fig. 4 Diffuse reflectance spectra (colored symbols) of (a)–(c) noncancerous and (d) and (e) cancerous human breast tissues over the range from 500 to 1600 nm, measured *ex vivo* with a fiber-probe-based setup and shown with fits of a diffusion theory model (black solid lines).[8] Differences between tissue types can be clearly seen and quantitatively related to changes in water and lipid volume fractions, which can then be employed for tissue classification. (Figure reproduced with permission.)

from adipose tissue, distinguishing invasive carcinoma from adipose, glandular, and fibroadenoma, and distinguishing DCIS from adipose tissue. The lipid volume fraction was statistically significant for distinguishing fibroadenoma from adipose tissue, distinguishing invasive carcinoma from adipose tissue, and distinguishing DCIS from adipose, fibroadenoma, and invasive carcinoma. The collagen volume fraction was statistically significant for distinguishing fibroadenoma from glandular tissue, distinguishing invasive carcinoma from adipose and fibroadenoma, and distinguishing DCIS from adipose tissue.

Olesberg et al.[25] employed a fiber-probe-based method to measure the absorbance of rat skin *in vivo* from 2000 to 2500 nm to optically measure glucose concentration. A tungsten-halogen light source coupled to a fiber probe with a ball lens was used for delivery of light to the skin. Photons that were transmitted through a fold in the animal's skin were detected by a second fiber probe, which sent the light to an InGaAs detector and a spectrometer. The absorption spectra were analyzed with a partial least squares model to determine spectral features that were related to glucose. This model was then employed to extract the change in glucose concentration in the skin over a 2-h period following venous delivery of glucose to the animal. The extracted magnitude (~5 mM at baseline to ~35-mM peak concentration following infusion) and temporal lineshape of the glucose concentration were found to be in good agreement (within ~15% at peak) with that obtained using a glucose analyzer.

Nishimura et al.[26] employed a time-resolved fiber-probe-based setup to measure absorption and reduced scattering coefficients from 1150 to 1520 nm in a human forearm *in vivo* (Fig. 5). The model fit to the data, using a water fraction in the neighborhood of 52% (a value in good agreement with that obtained using magnetic resonance imaging), was accurate from 1150 to 1350 nm. However, the fit was notably worse at wavelengths of 1400 nm and longer; to explain this discrepancy, the authors suggest that their diffusion-based model was likely inaccurate in this region, partly because absorption from water is so high in this range that the photon paths cannot be considered to be diffuse. In a proof-of-principle study, Bargigia et al.[27] used a fiber probe to obtain time-resolved spectroscopic measurements of porcine fat *ex vivo* from 1100 to 1700 nm, observing 1200-, 1400-, and 1700-nm lipid absorption peaks and a reduced scattering coefficient with values in the 1 to 4 cm^{-1} range from 1100 to 1700 nm. Taroni et al.[28] obtained the time-resolved *in vivo* reflectance of human breast tissue from 900 to 1300 nm, reporting an absorption peak around 1200 nm containing contributions from water, lipids, and collagen.

The main conclusions of the fiber-probe-based SWIR studies were: (1) fiber-probe configurations enable SWIR measurements of intact biological tissues, both *in vivo* and *ex vivo*, (2) adding the SWIR range to these measurements enables more accurate extraction[21] of water and lipid volume fractions than similar measurements over only the VIS-NIR range, and (3) the water and lipid content obtained from fiber-based SWIR measurements show some promises in enabling accurate classification of diseased tissues; for instance, distinguishing vulnerable atherosclerotic plaque from stable plaque[22,23] and distinguishing different types of breast cancer from nonmalignant breast tissues.[8]

4 Short-Wave Infrared Imaging

SWIR methods have recently been employed for imaging applications.[9,29,30] Imaging techniques provide several advantages over fiber-probe-based methods; specifically, they enable noncontact measurement of *in vivo* or *ex vivo* tissues and provide information from fields of view that may be up to tens of centimeters in both the *x*- and *y*-dimensions.

Allen et al.[9] performed *ex vivo* spectroscopic photoacoustic imaging of human aorta with plaques from 740 to 1400 nm, also imaging a plaque buried beneath 2.8 mm of blood to demonstrate *in vivo* feasibility. The authors of Ref. 9 cited SWIR

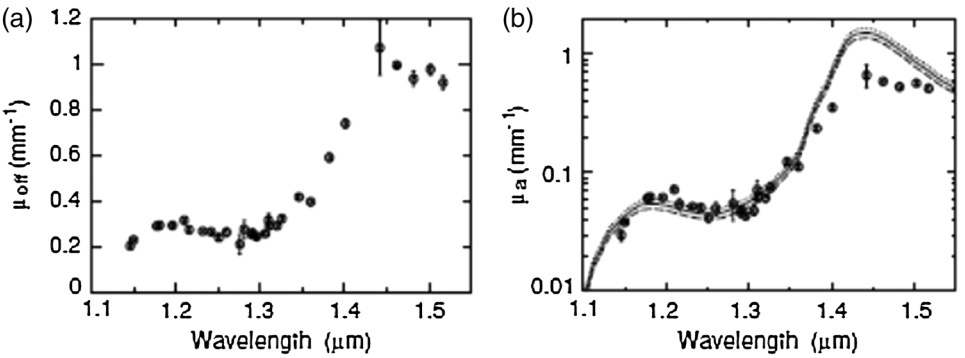

Fig. 5 (a) Effective attenuation, $\mu_{\text{eff}}(\lambda)$ and (b) absorption, $\mu_a(\lambda)$ coefficients of a human forearm *in vivo*, from 1150 to 1520 nm, obtained from time-resolved reflectance with a fiber probe.[26] The measured μ_a values in (b) are shown alongside models for $\mu_a(\lambda)$ using water fractions of 47%, 52%, and 57%, represented with the broken line, solid line, and dotted line, respectively, employing the water absorption spectrum from Ref. 4. The water fraction of 52% was in good agreement with that obtained for muscle tissue using magnetic resonance imaging. This result suggests that the time-resolved SWIR imaging has the potential to quantitatively and noninvasively sense water content beneath the tissue surface *in vivo*.

photoacoustic imaging as a potential means of providing improved diagnosis of vulnerable plaque, due to its ability to interrogate structure and function of tissue with a high sensitivity to lipid absorption features in the SWIR wavelength range.

Fleming et al.[14] performed spectroscopic optical coherence tomography (OCT) with a system designed for use through a catheter,[38] to image tissue phantoms with lipid emulsion inclusions (representing coronary plaques) injected ~1 mm beneath the surface of porcine aortic tissue. The center wavelength and bandwidth of the OCT system were 1300 and 100 nm, respectively; therefore, the system acquired data from 1250 to 1350 nm. The spectral data and OCT images were employed to generate probability maps for collagen and cholesterol beneath the surface of the phantom. The plaques were detected as regions with a higher probability of cholesterol and a lower probability of collagen, relative to the surrounding medium. The cholesterol inclusion was clearly visible in a region beneath 0.79 mm of aortic tissue, but it was not visible beneath 1.17 mm of tissue. This study suggests that the multispectral SWIR imaging has the potential to distinguish spectral signatures of cholesterol and collagen for diagnosis of arterial plaque.

To test the ability of SWIR wavelengths to noninvasively interrogate biological tissues, Cao et al.[29] measured transmitted intensity of *ex vivo* murine skeletal muscle, liver, kidney, cardiac tissue, cerebrum, cerebellum, and adipose tissues as a function of wavelength from 800 to 1450 nm. Cao et al.[29] also performed SWIR transmittance imaging from 800 to 1400 nm through the head of a mouse *in vivo*, using the ratio of measured intensities at 1075 and 975 nm as a contrast metric, to demonstrate the potential of NIR/SWIR methods to provide an image of the skull that could be coregistered, in terms of gross anatomy, with images that were obtained by x-ray.

Akbari et al.[39] used a hyperspectral VIS-NIR-SWIR imaging system for detection and monitoring of intestinal ischemia *in vivo* in a porcine model. The instrumentation included two halogen lamps for illumination and two cameras (a 400- to 1000-nm camera and a 900- to 1700-nm camera) for image detection. The SWIR (900 to 1700 nm) camera provided a spectral resolution of 5 nm by use of a 30-m slit. The slit provided one thin "slice" of the (x, y, λ) image at a time, so the slit was scanned across the object using a "push-broom" method to obtain the entire wide-field image. Images were obtained for 157 wavelength bands in the 900- to 1700-nm range; each image took ~15 s to acquire and the spatial resolution of the images was ~0.35 mm/pixels. In the ischemia experiment, a clamping procedure was performed on a portion of the intestine and the associated blood vessels. Wide-field reflectance images of the exposed abdominal cavity, with peritoneum, spleen, intestine, and bladder within the field of view, were acquired intraoperatively before clamping and ~2, ~4, and ~6 min after clamping. The reflectance data were analyzed with a quantitative, feature-based method, in order to locate spectral regions in which the lineshape measured from ischemic tissue was the most notably different than that measured from normal tissue. To accomplish this, the derivative of the reflectance spectrum was evaluated at each wavelength, and the absolute value of the sum of these derivatives was calculated for different subsets of the measured wavelength range. It was found that the range from 999 to 1182 nm was optimal for distinguishing ischemic spectra from normal spectra, so the magnitude of the sum of the derivatives in this region was defined to be the ischemia index. Camera pixels with ischemia index values that surpassed a specific threshold were labeled as ischemic. Using the SWIR images, the regions of ischemia were classified with a false positive rate of 8% and a false negative rate of 7%. Akbari et al.[40] also performed a similar study on freshly excised human gastric tumors, using the same technology as in Ref. 39. With a mathematical approach similar to that employed in Ref. 39, a "cancer index" was calculated by summing the square of the reflectance derivative from 1226 to 1251 nm and the square of the reflectance derivative from 1288 to 1370 nm. Despite being based purely on mathematical differences in spectral lineshape instead of biophysical tissue optics parameters, the model distinguished cancerous tissues from noncancerous tissues with a false positive rate of 7% and a false negative rate of 9%. Furthermore, the method showed potential for detecting tumors buried beneath up to ~2 to 3 mm of benign mucosal tissue.

Randeberg et al.[41] employed an SWIR imaging system to assess human skin bruises. The instrument acquired images in 160 spectral bands from 900 to 1700 nm. The study

determined that the 958-nm image was best for distinguishing vasculature, but the 1584-nm image was best for distinguishing the bruise from the surrounding tissue. In a subsequent study, Randeberg and Hernandez-Palacios[42] employed an SWIR imager that spanned the 950- to 2500-nm range with 256 spectral bands and 6-nm spectral sampling to image and characterize skin bruises. A minimum noise transform was employed to enhance the qualitative features of the measured SWIR spectra. The images at 1250, 1443, and 2165 nm were employed to construct false-color "RGB" maps of the bruises. The SWIR absorption contrast (attributed to increased water concentration in the bruise due to edema) was found to provide better distinction of bruised tissue than the VIS-NIR absorption contrast (attributed to local changes in blood content). These results suggest that SWIR imaging could provide notable improvement in characterization of bruises relative to visual inspection of the color of the bruise, which is the current clinical gold standard for bruise assessment.[41–44]

Recently, *in vivo* wide-field SWIR imaging of burns in a rat model was performed using a hybrid approach involving both spatially modulated and unstructured (homogeneous) illuminations.[30] This method enabled the separation of absorption and reduced scattering coefficients over a wide (850 to 1800 nm) wavelength range (Fig. 6), showing potential to distinguish burn-related changes in tissue absorption and scattering in the SWIR regime. The measured tissue absorption and reduced scattering coefficients obtained from this study were also input into a Monte Carlo model[45] to obtain reflectance and transmittance spectra from 850 to 1800 nm (Fig. 7). The reflectance and transmittance curves in Fig. 7 illustrate that, in spite of the decreased scattering in the SWIR regime relative to the NIR, there are still some SWIR wavelengths (most notably from 1400 to 1500 nm) that have very low transmittance due to the high absorption coefficient of water in that range of wavelengths.

The main conclusions of the SWIR imaging studies were: (1) the SWIR regime provides sufficient optical penetration depth (e.g., up to ~5 mm for 1100 nm photons, using the equation employed in Ref. 19) to interrogate subsurface tissue features, such as changes in vasculature and collagen structure in burns and cancerous tissues, in a noninvasive manner over a wide (tens of centimeters)^2 field of view, and (2) the enhanced absorption contrast from water and lipid in the SWIR regime (relative to the VIS-NIR) provides the potential for quantitative wide-field mapping of changes in tissue chromophore concentrations in perturbed (e.g., burned and diseased) tissues.

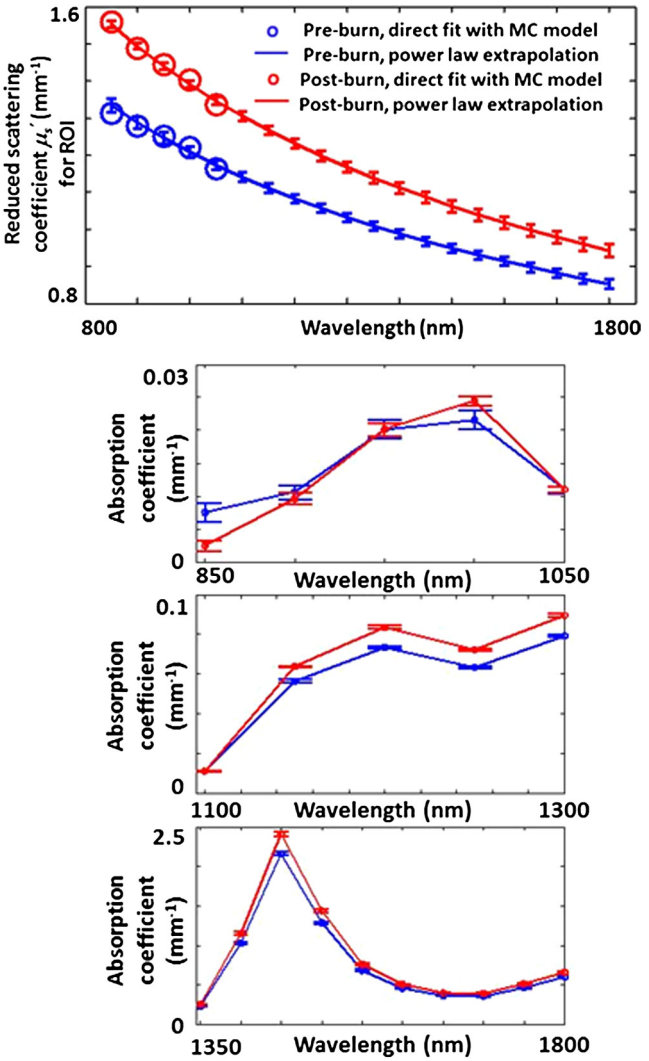

Fig. 6 Reduced scattering (top panel) and absorption (three bottom panels) coefficients from 850 to 1800 nm obtained for *in vivo* rat tissue preburn and ~2-h postburn using a hybrid wide-field imaging method with spatially modulated and unmodulated light.[30] (Figure reproduced with permission).

5 Discussion and Conclusions

SWIR measurements of biological tissues are capable of detecting changes in absorption from chromophores such as water [absorption peaks at 1150, 1450, 1900 nm (Refs. 4 and 8)] and lipids [absorption peaks at 930, 1040, 1200, 1400, and 1700 nm (Refs. 5, 7, and 8)], as well as possibly collagen [absorption peaks at 1200 and 1500 nm (Ref. 8)]. For each of these tissue constituents, prominent spectral characteristics like those observed in the SWIR regime are not present in the VIS-NIR, suggesting that SWIR spectroscopy and imaging techniques provide potential for enabling a more information-rich means of tissue diagnostics and characterization.

Thus far, many SWIR tissue optics studies might generally be described as exploratory and "proof-of-principle" in nature. The current state-of-the-art has primarily demonstrated that (1) SWIR tissue optics techniques have been employed to access spectral bands that are generally related to water and lipid content, and (2) employing the SWIR enables extraction of an expanded set of tissue parameters that may be useful for disease detection, classification, characterization, and monitoring. Additional research needs to be performed in order to quantitatively assess the value of expanding existing instrumentation into the SWIR range in terms of improved diagnostic capability.

One of the reasons that SWIR has seen relatively limited application in the biomedical sector up until recently is that InGaAs sensor arrays,[46] which are often used for SWIR detection, have been cost prohibitive. However, recent technological advances, coupled with an increase in the number of companies supplying this technology, have enabled a drop in price of roughly an order of magnitude over the time period from 2010 to 2014. In addition, access to high-resolution InGaAs sensor arrays has been limited by various national defense-related policies such as International Traffic in Arms Regulations. An increased supply of affordable SWIR sensing instrumentation has the potential to enable more widespread SWIR-oriented biomedical optics research and development.

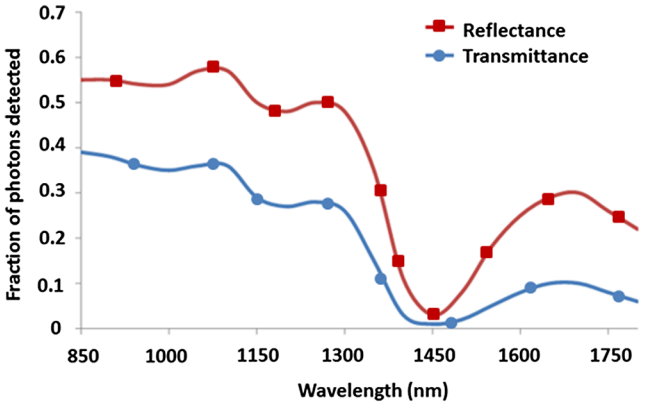

Fig. 7 Reflectance and transmittance of rat skin in the SWIR range, calculated using Monte Carlo simulation.[45] The absorption and reduced scattering coefficients input into the simulations are those shown in Fig. 6 for normal rat tissue *in vivo*, as obtained from multispectral SWIR imaging.[30] These reflectance and transmittance curves indicate that although scattering decreases monotonically over the SWIR regime, the mean penetration depth of the light does not increase monotonically as a result. Instead, the SWIR penetration depth curve for skin exhibits a number of local maxima and minima that coincide with the absorption features of water in this wavelength range.

Two examples of application areas in which there has been notable activity with a potential to exploit the SWIR regime are the identification of vulnerable atherosclerotic plaque and classification of stages of malignancy in breast cancer.

SWIR applications related to atherosclerosis show specific promise because several studies have shown that the lipid absorption information in this range can potentially distinguish vulnerable plaque.[9,14,22,23] For eventual *in vivo* translation, the SWIR provides an advantage over the VIS-NIR for detecting changes in lipids amidst a high concentration of blood (which absorbs much less prominently in the SWIR than in the VIS-NIR). In fact, one group has already employed these concepts to design a clinically compatible instrument for plaque detection that accesses the SWIR portion of the spectrum.[47–49] This example has been successfully translated into a commercial product, the catheter-based TVC Imaging System developed by Infraredx®, for determining information about the structure and plaque content of blood vessels *in vivo*.[50]

SWIR applications related to breast cancer classification are also particularly promising because previous NIR studies have already shown that water and lipid content are of great potential use in distinguishing breast cancer,[51,52] and another study has shown that including SWIR wavelengths can enable extraction of water and lipid volume fractions with a factor of four increase in confidence level relative to those obtained using only VIS-NIR light, by employing the enhanced absorption contrast from these tissue components in the SWIR.[21]

Additional biomedical applications of SWIR technology include quantitative sensing of biophysical tissue property changes in burn wounds (employing the increased sensitivity of SWIR wavelengths to absorption features from water, enabling detection of edema in burned tissue)[30] and detection of changes in glucose concentration (if the spectral range is extended out to 2500 nm).[25] The applications described in this paper illustrate the potential of SWIR tissue optical spectroscopy and imaging to provide enhanced diagnostic information.

The scattering of biological tissue has been shown to follow a power-law model over the VIS-NIR-SWIR regimes, and the absorption of tissue has many distinctive spectral features in the SWIR. Therefore, employing SWIR wavelengths can potentially enable interrogation of many different photon penetration depths within the tissue. Layered tissues, such as skin, have different absorption and scattering properties in each layer due to the heterogeneity of tissue morphology and chromophore concentration. As a result, the ability to interrogate different depths may be particularly helpful for characterizing layered tissues such as skin.

Incorporating the SWIR wavelength region into tissue optics measurements can potentially help to improve *in vivo* tissue characterization. In the VIS-NIR regime, tissue absorption is primarily attributed to hemoglobin, which exhibits strong spectral peaks near 420, 540, and 577 nm. However, in the SWIR, absorption from hemoglobin is multiple orders of magnitude lower than in the VIS-NIR, while the SWIR absorption peaks of water and lipid are typically at least an order of magnitude greater than those at the far edge of the NIR. Therefore, for *in vivo* optical spectroscopy and imaging studies, where tissue is interrogated with a probe attached to an endoscope or a catheter, the detected SWIR signal will be largely unaffected by the presence of blood in the imaged field. In addition, the signal will be much more sensitive to water and lipids than it would be in the VIS-NIR. As a result, SWIR wavelengths may provide valuable subsurface information about the water and lipid content of human tissues *in vivo*. This information can potentially assist in the detection, characterization, and classification of conditions such as cancer and atherosclerosis. In fact, it has already been shown that water and lipid absorptions provide useful diagnostic "fingerprints" for detection of both cancer[8,40] and atherosclerosis.[9,14,22,23,47–49]

On the path toward a more widespread implementation of SWIR tissue optics measurements, one important factor to consider is the temperature dependence of tissue absorption features in the SWIR regime. Water is a primary SWIR absorber in tissue, and it has been shown[53,54] that the spectral location of SWIR water absorption peaks can vary with temperature. Jansen et al.[53] reported a water absorption coefficient that decreased with increasing temperature and a water absorption peak that shifted from 1940 nm at 22°C to 1920 nm at 70°C. Kakuta et al.[54] reported a blue shift in the 1450 nm water absorption peak when the temperature was varied between 24°C and 40°C. Furthermore, temperature-dependent changes in the measured optical properties of skin have been reported in the VIS-NIR,[55,56] a finding that suggests that such changes are likely expected in the SWIR as well. The results in Refs. 55 and 56 were cited by Troy and Thennadil[18] as motivation for performing all their SWIR integrating sphere measurements of skin tissue at body temperature (37°C). Temperature-dependent shifts in the SWIR tissue absorption peaks can potentially be reduced or eliminated through careful control of temperature, or if such control is not possible, the locations of the peaks can potentially be reshifted by calibrating the SWIR instrumentation through measurements of tissue constituents (e.g., water and lipid) as a function of temperature and using this calibration to correct the peak locations in a postprocessing routine.

In conclusion, the application of SWIR-based optical spectroscopy and imaging to *in vivo* tissue has, to date, been relatively limited. Studies suggest that this wavelength range has potential for enhancing the current state-of-the-art in tissue optics measurements, which, at present, typically only employ light in the VIS-NIR spectral range. This enhancement is

primarily provided by increased sensitivity to endogenous tissue components (such as water, lipids, and collagen) that absorb light prominently in the SWIR but do not have strong absorption in the VIS-NIR. Incorporating SWIR detection into biomedical optics technologies has the potential to provide additional information regarding tissue composition and function and as such may be useful for enhanced tissue assessment and classification.

Acknowledgments

R.H.W. was supported by a postdoctoral fellowship from the Hewitt Foundation for Medical Research. K.P.N. was supported by the NSF IGERT (Grant 1144901), "Biophotonics across Energy, Space, and Time." F.B.J. was internally funded by Raytheon Vision Systems. Additional support is provided by the National Institutes of Health (NIH-R21EB014440 and NIH-R21NS078634), the NIH/NIBIB funded LAMMP (P41EB015890), the Military Medical Photonics Program (FA9550-10-1-0538), and the Arnold and Mabel Beckman Foundation.

References

1. T. D. O'Sullivan et al., "Diffuse optical imaging using spatially and temporally modulated light," *J. Biomed. Opt.* **17**(7), 071311 (2012).
2. J. Q. Brown et al., "Advances in quantitative UV-visible spectroscopy for clinical and pre-clinical application in cancer," *Curr. Opin. Biotechnol.* **20**(1), 119–131 (2009).
3. S. Prahl, *Optical Absorption of Hemoglobin*, Oregon Medical Laser Center, Portland, OR, omlc.ogi.edu/spectra/hemoglobin (9 March 2015).
4. G. M. Hale and M. R. Querry, "Optical constants of water in the 200 nm to 200 μm wavelength region," *Appl. Opt.* **12**(3), 555–563 (1973).
5. R. L. P. van Veen et al., "Determination of VIS-NIR absorption coefficients of mammalian fat, with time and spatially resolved diffuse reflectance and transmittance spectroscopy," in *OSA BIOMED Topical Meeting*, Miami Beach, FL (2004).
6. J. Q. Nguyen et al., "Spatial frequency domain imaging of burn wounds in a preclinical model of graded burn severity," *J. Biomed. Opt.* **18**(6), 066010 (2013).
7. G. B. Altshuler, R. R. Anderson, and D. Manstein, "Method and apparatus for the selective targeting of lipid-rich tissue," United States Patent, Patent No. 6,605,080 B1 (2003), http://www.npsg.uwaterloo.ca/data/skin/lipid_absorption.m (9 March 2015).
8. R. Nachabé et al., "Diagnosis of breast cancer using diffuse optical spectroscopy from 500 to 1600 nm: comparison of classification methods," *J. Biomed. Opt.* **16**(8), 087010 (2011).
9. T. J. Allen et al., "Spectroscopic photoacoustic imaging of lipid-rich plaques in the human aorta in the 740 to 1400 nm wavelength range," *J. Biomed. Opt.* **17**(6), 061209 (2012).
10. H. M. Monavar et al., *Evaluation of the Potential of Near-Infrared (NIR) Spectroscopy for Predicting Fatty Acid Composition of Sturgeon's Caviars*, SpectroscopySolutions, 2013, http://www.spectroscopy-solutions.org/ (9 March 2015).
11. P. Wang et al., "Mapping lipid and collagen by multispectral photoacoustic imaging of chemical bond vibration," *J. Biomed. Opt.* **17**(9), 096010 (2012).
12. S. S. Nielsen, *Food Analysis*, 4th ed., Springer, New York (2010).
13. P. Wang et al., "Bond-selective imaging of deep tissue through the optical window between 1600 and 1850 nm," *J. Biophotonics* **5**(1), 25–32 (2012).
14. C. P. Fleming et al., "Depth resolved detection of lipid using spectroscopic optical coherence tomography," *Biomed. Opt. Express* **4**(8), 1269–1284 (2013).
15. Y. Du et al., "Optical properties of porcine skin dermis between 900 nm and 1500 nm," *Phys. Med. Biol.* **46**(1), 167–181 (2001).
16. E. Zamora-Rojas et al., "Optical properties of pig skin epidermis and dermis estimated with double integrating spheres measurements," *Innovative Food Sci. Emerging Technol.* **20**, 343–349 (2013).
17. E. Zamora-Rojas et al., "Double integrating sphere measurements for estimating optical properties of pig subcutaneous adipose tissue," *Innovative Food Sci. Emerging Technol.* **19**, 218–226 (2013).
18. T. L. Troy and S. N. Thennadil, "Optical properties of human skin in the near infrared wavelength range of 1000 to 2200 nm," *J. Biomed. Opt.* **6**(2), 167–176 (2001).
19. A. N. Bashkatov et al., "Optical properties of human skin, subcutaneous and mucous tissues in the wavelength range from 400 to 2000 nm," *J. Phys. D* **38**(15), 2543–2555 (2005).
20. M. Friebel et al., "Influence of oxygen saturation on the optical scattering properties of human red blood cells in the spectral range 250 to 2,000 nm," *J. Biomed. Opt.* **14**(3), 034001 (2009).
21. R. Nachabé et al., "Estimation of biological chromophores using diffuse optical spectroscopy: benefit of extending the UV-VIS wavelength range to include 1000 to 1600 nm," *Biomed. Opt. Express* **1**(5), 1432–1442 (2010).
22. J. Wang et al., "Near-infrared spectroscopic characterization of human advanced atherosclerotic plaques," *J. Am. Coll. Cardiol.* **39**(8), 1305–1313 (2002).
23. P. R. Moreno et al., "Detection of lipid pool, thin fibrous cap, and inflammatory cells in human aortic atherosclerotic plaques by near-infrared spectroscopy," *Circulation* **105**(8), 923–927 (2002).
24. R. Nachabé et al., "Estimation of lipid and water concentrations in scattering media with diffuse optical spectroscopy from 900 to 1,600 nm," *J. Biomed. Opt.* **15**(3), 037015 (2010).
25. J. T. Olesberg et al., "In vivo near-infrared spectroscopy of rat skin tissue with varying blood glucose levels," *Anal. Chem.* **78**(1), 215–223 (2006).
26. G. Nishimura, I. Kida, and M. Tamura, "Characterization of optical parameters with a human forearm at the region from 1.15 to 1.52 μm using diffuse reflectance measurements," *Phys. Med. Biol.* **51**(11), 2997–3011 (2006).
27. I. Bargigia et al., "Time-resolved diffuse optical spectroscopy up to 1700 nm by means of a time-gated InGaAs/InP single-photon avalanche diode," *Appl. Spectrosc.* **66**(8), 944–950 (2012).
28. P. Taroni et al., "First in vivo spectral characterization of breast up to 1300 nm," *Proc. SPIE* **7896**, 78962L (2011).
29. Q. Cao et al., "Multispectral imaging in the extended near-infrared window based on endogenous chromophores," *J. Biomed. Opt.* **18**(10), 101318 (2013).
30. R. H. Wilson et al., "Quantitative short-wave infrared multispectral imaging of in vivo tissue optical properties," *J. Biomed. Opt.* **19**(8), 086011 (2014).
31. J. W. Pickering et al., "Double-integrating-sphere system for measuring the optical properties of tissue," *Appl. Opt.* **32**(4), 399–410 (1993).
32. R. A. Ryerson, Ed., *Remote Sensing for the Earth Sciences*, John Wiley & Sons, New York (1999).
33. A. Roggan and G. Müller, Eds., *Laser-Induced Interstitial Thermotherapy*, SPIE, Bellingham, Washington (1995).
34. R. R. Anderson et al., "Selective photothermolysis of lipid-rich tissues: a free electron laser study," *Lasers Surg. Med.* **38**(10), 913–919 (2006).
35. J. A. Parrish and R. R. Anderson, "Selective photothermolysis: precise microsurgery by selective absorption of pulsed radiation," *Science* **220**(4596), 524–527 (1983).
36. K. Martin, "In vivo measurements of water in skin by near-infrared reflectance," *Appl. Spectrosc.* **52**(7), 1001–1007 (1998).
37. H. Arimoto, M. Egawa, and Y. Yamada, "Depth profile of diffuse reflectance near-infrared spectroscopy for measurement of water content in skin," *Skin Res. Technol.* **11**(1), 27–35 (2005).
38. S. H. Yun et al., "Comprehensive volumetric optical microscopy in vivo," *Nat. Med.* **12**(12), 1429–1433 (2006).
39. H. Akbari, K. Kojima, and N. Tanaka, "Detection and analysis of the intestinal ischemia using visible and invisible hyperspectral imaging," *IEEE Trans. Biomed. Eng.* **57**(8), 2011–2017 (2010).
40. H. Akbari et al., "Cancer detection using infrared hyperspectral imaging," *Cancer Sci.* **102**(4), 852–857 (2011).
41. L. L. Randeberg et al., "Hyperspectral imaging of bruised skin," *Proc. SPIE* **6078**, 60780O (2006).
42. L. L. Randeberg and J. Hernandez-Palacios, "Hyperspectral imaging of bruises in the SWIR spectral region," *Proc. SPIE* **8207**, 82070N (2012).
43. N. E. I. Langlois and G. A. Gresham, "The aging of bruises: a review and study of the colour changes with time," *Forensic Sci. Int.* **50**, 227–238 (1991).

44. S. Maguire et al., "Can you age bruises accurately in children? A systematic review," *Arch. Dis. Child.* **90**, 187–189 (2005).
45. L. Wang, S. L. Jacques, and L. Zheng, "Monte Carlo modeling of photon transport in multi-layered tissues," *Comput. Methods Programs Biomed.* **47**, 131–146 (1995).
46. R. M. Schols et al., "Automated spectroscopic tissue classification in colorectal surgery," *Surg. Innovation* **23** (2015).
47. S. Waxman, F. Ishibashi, and J. D. Caplan, "Rationale and use of near-infrared spectroscopy for detection of lipid-rich and vulnerable plaques," *J. Nucl. Cardiol.* **14**(5), 719–728 (2007).
48. C. M. Gardner et al., "Detection of lipid core coronary plaques in autopsy specimens with a novel catheter-based near-infrared spectroscopy system," *JACC Cardiovasc. Imaging* **1**(5), 638–648 (2008).
49. J. A. Goldstein et al., "Detection of lipid-core plaques by intracoronary near-infrared spectroscopy identifies high risk of periprocedural myocardial infarction," *Circ. Cardiovasc. Interv.* **4**(5), 429–437 (2011).
50. Infraredx(R), http://www.infraredx.com/ (9 March 2015).
51. P. Taroni et al., "Clinical trial of time-resolved scanning optical mammography at 4 wavelengths between 683 and 975 nm," *J. Biomed. Opt.* **9**(3), 464–473 (2004).
52. A. Cerussi et al., "In vivo absorption, scattering, and physiologic properties of 58 malignant breast tumors determined by broadband diffuse optical spectroscopy," *J. Biomed. Opt.* **11**(4), 044005 (2006).
53. E. D. Jansen et al., "Temperature dependence of the absorption coefficient of water for midinfrared laser radiation," *Lasers Surg. Med.* **14**(3), 258–268 (1994).
54. N. Kakuta et al., "Temperature imaging of sub-millimeter thick water using a near infrared camera," *Int. J. Heat Mass Transfer* **52**(19–20), 4221–4228 (2009).
55. T. L. Troy, D. L. Page, and E. M. Sevick-Muraca, "Optical properties of normal and diseased breast tissues: prognosis for optical mammography," *J. Biomed. Opt.* **1**(3), 342–355 (1996).
56. J. Laufer et al., "Effect of temperature on the optical properties of ex vivo human dermis and subdermis," *Phys. Med. Biol.* **43**(9), 2479–2489 (1998).

Biographies of the authors are not available.